Nanoscale structural disorder in manganese oxide particles embedded in Nafion†

Shery L. Y. Chang,[a,b‡*] Archana Singh,[a] Rosalie K. Hocking,[c] Christian Dwyer,[b] and Leone Spiccia[a*]

Received Xth XXXXXXXXXX 20XX, Accepted Xth XXXXXXXXX 20XX

First published on the web Xth XXXXXXXXXX 200X

DOI: 10.1039/b000000x

Earlier studies have shown that manganese oxide particles derived from a manganese molecular complex embedded in Nafion film have one order of magnitude higher water-oxidation catalytic activity per manganese compared to many unsupported solid-state manganese oxide particles. Using transmission electron microscopy and electron scattering simulations, we have shown that the sodium-birnessite phase particles in Nafion exhibit an exceptionally high degree of the layer mis-registration, and a high concentration of Mn vacancies, compared to the synthetic birnessite nanoparticles. It is therefore proposed that the differences in the activities correlate with the degree of disorder in the manganese oxide particles.

Solar-driven water splitting, where a combination of water oxidation and proton reduction is used to generate hydrogen fuel, is poised to provide renewable energy without greenhouse emissions. A major challenge in achieving this process lies in the requirement of a significant overpotential to drive the four-electron process of water oxidation. Hence, considerable efforts have been devoted to reduce this overpotential through the development of efficient catalysts.

Inspired by the highly-active, naturally-occurring manganese cluster ($CaMn_4O_5$)[1] of the water-oxidizing complex of photosystem II (PSII-WOC), the development of catalysts containing inexpensive and earth-abundant manganese has attracted vast interest[2–4] (as have other transition metal elements[5–9]). In particular, manganese oxides with oxidation states between Mn^{III} and Mn^{IV} have been demonstrated to exhibit catalytic activity under alkaline conditions[10–13], and activities under mild conditions have also been reported recently[14–17] .

Manganese oxides are known to have a large number of polymorphs, a number of which have been reported to be active for water oxidation. For example, nanostructured α-MnO_2, β-MnO_2 and screen-printed β-MnO_2 film have been found active in photo-electrochemical systems[18,19], and nanoparticulate Mn_2O_3[20], δ-MnO_2[16,21–23] and λ-MnO_2[24] have also been reported to be active in neutral to alkaline conditions. Recently, it was proposed that amorphous-structured manganese oxides can be more active compared to crystalline phases in neutral conditions[17,25]. However, there has been significant ambiguities in determining the catalytic active components in these nano-structured systems. In addition, the presence of structural disorders in the materials, such as vacancies or lattice strain, can result in significant changes to local electronic structure and hence alter their catalytic properties[26]. Moreover, such effects are often more pronounced in nanoparticles. Such observations would explain why, for some manganese oxides of the same phase, such as δ-MnO_2, there exists a broad deviation in the reported activity under similar reaction conditions[14–16,25]. These examples demonstrate the importance of acquiring a detailed understanding of the type of structural disorder in nanoparticulate manganese oxides.

Here, we present a detailed structural study of the manganese oxide particles formed in Nafion film under active water oxidation conditions, using transmission electron microscopy (TEM) techniques. Utilising the strong interaction between the beam electrons and the sample, TEM is well-suited for studying structural disorder in embedded nanoparticulate manganese oxide, where the particle concentration and size can be too low for reliable characterisation using typical spectroscopy and X-ray diffraction methods. The combination of TEM imaging and diffraction techniques over spectroscopy alone gives advantages that imaging offers direct information on the morphological changes, while the coherent diffraction intensities derived from the selected-area patterns allow us to easily differentiate the structural phases and also provide information on the degree of structural order. In ad-

† Electronic Supplementary Information (ESI) available: [Details of materials synthesis method, TEM specimen preparation procedures of manganese oxides in Nafion, catalytic activity testing, detailed description of TEM imaging, electron diffraction and energy dispersive spectroscopy techniques, comparisons of simulated electron diffraction pattern of various manganese oxide phases; and electron scattering simulations of structural disorder in manganese oxide.]. See DOI: 10.1039/b000000x/

[a] *School of Chemistry, Monash University, Clayton, Australia.*

[b] *Ernst Ruska-Centrum and Peter Gruenberg Institute, Forschungszentrum Juelich, Germany.*

[c] *School of Pharmacy and Molecula Science, Discipline of Chemistry, James Cook University, Townsville, Australia.*

∗ To whom correspondence should be addressed. E-mail:shery.chang@fz-juelich.de and leone.spiccia@monash.edu

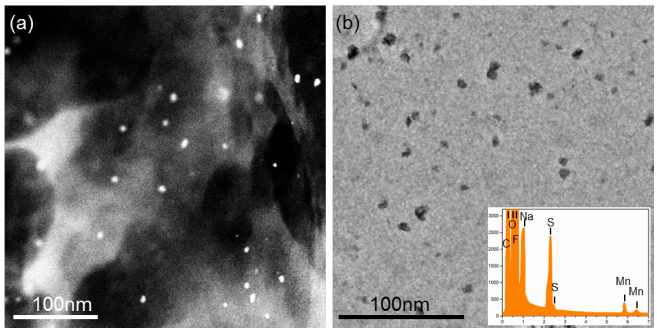

Fig. 1 Low magnification ADF-STEM image (a) and BF-TEM images (b) of the manganese oxide particles, derived from Mn^{III} dimer complex in Nafion film. Inset shows the EDS spectra of the area focused around nanoparticles.

dition, the electron scattering simulations were applied to explain the origin of the structural disorder observed in the electron diffraction of the manganese oxide particles in Nafion films.

Manganese oxide particles embedded in Nafion films were generated by electro-oxidation of the Nafion films doped with the manganese complex precursor, $[(Me_3TACN)_2Mn^{III}_2(\mu\text{-}O)(\mu\text{-}CH_3COO)_2]^{2+}$, following a procedure reported previously [16]. This system has been shown to exhibit a much higher turnover frequency (TOF) per Mn site compared to many electro-deposited solid-state MnO_x, such as birnessite-phase catalysts, at near neutral conditions (41 - 44 $Mn^{-1}h^{-1}$ v.s. 0.2 - 1.2 $Mn^{-1}h^{-1}$) [16,27] (details of the catalytic activity test can be found in the Supporting Information). In order to avoid damage while transferring the film onto a TEM grid for observation, the doped films were prepared directly onto carbon-coated gold TEM grids. Details of materials synthesis and preparation can be found in Supporting Information. Fig. 1(a) shows an ADF-STEM image of manganese oxide particles in Nafion. It can be seen that the particles (the bright spheres) are well-dispersed in the Nafion film (the varying background contrast), which has the characteristic interconnected network with holey features. The bright-field TEM image shown in Fig. 1(b) provides a similar observation, with the particles (dark spheres) appearing against the grey-background of the Nafion film. Energy dispersive x-ray spectra (EDX), obtained using a focused beam from areas containing nanoparticle areas (inset), exhibits a weak Mn signal and strong C, O, F and S signals, confirming that the manganese-containing particles are embedded in a significantly thick layer of Nafion film.

In order to determine the phase and possible structural disorder of manganese oxide particles, selected-area electron diffraction has been applied. However, as the relatively low concentration of particles are embedded in the thick Nafion film, the diffraction intensities from nanoparticles can be weak compared to those from Nafion. In addition, the structural

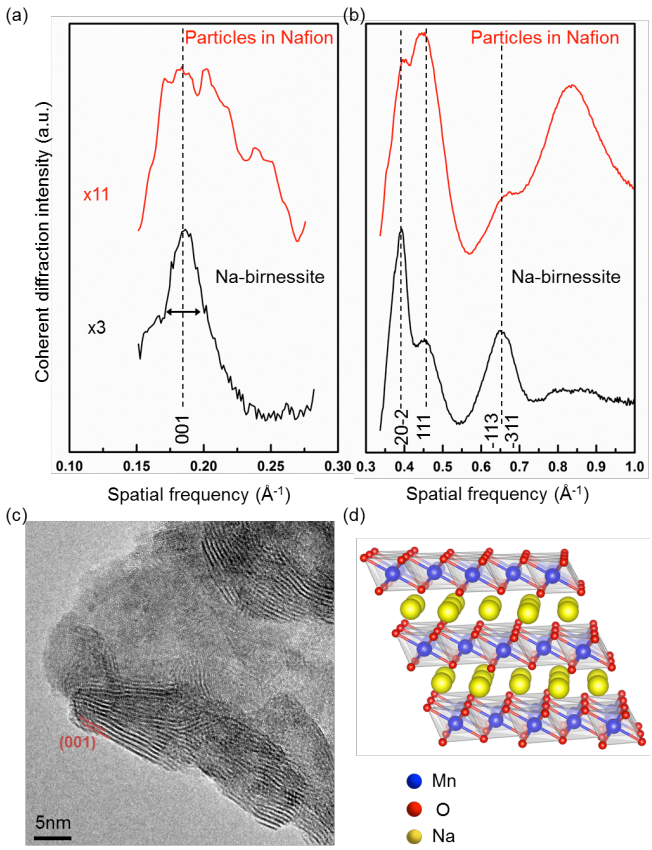

Fig. 2 Coherent diffraction intensities of the manganese oxide particles in Nafion, and the synthetic Na-birnessite (a)-(b). (In the case of (a), the low spatial frequencies (<0.3 $Å^{-1}$) has been magnified for better visibility.) (c) HRTEM image of the synthetic Na-birnessite; (d) Atomic model showing layered structure of monoclinic Na-birnessite.

disorder of nanoparticles is manifest in the shape and intensity of the diffraction peaks. Therefore, we have extracted the coherent diffraction intensity (CDI) from the selected-area diffraction patterns to obtain the structural details of the particles. CDI is more sensitive to the weak diffraction intensities and is therefore able to provide information from a small number of particles within a thick matrix. Fig. S2 shows the CDI of the manganese oxide particles in the Nafion. For comparison, the Nafion film manganese precursor doped before electro-oxidation is also shown in the figure. The coherent diffraction intensity in Fig. S2(c) shows three additional narrower peaks (red line labelled with arrows) superimposed on the broad peaks that closely resemble those of doped Nafion *before* applying potential. This observation is consistent with the formation of manganese oxide particles.

To elucidate the structural disorder of the Nafion-embedded manganese oxide particles, we have compared their CDI with

that from the well-characterised synthetic manganese oxide (Na-birnessite) particles, as shown in Fig. 2. The structural phase of the embedded particles has also been confirmed as the dehydrated monoclinic Na-birnessite structure[28], by comparisons with the simulated electron diffraction intensities from a range of manganese oxide single crystal phases (see Fig. S3). Further comparison on the coherent diffraction intensity of the manganese oxide particles in Nafion and the synthetic Na-birnessite reveals some important features, as shown in Fig. 2. Firstly, the diffraction peaks appear to be broadened, occurring for both the embedded particles and the synthetic birnessite. It can be seen in Fig. 2 that the broadening results in only four visible peaks between 0.3-1 $Å^{-1}$. Secondly, the (001) peak of the embedded particles shown in Fig. 2(a) is very weak, having a height of only about 10% relative to the strongest peak, whereas the theoretical (001) peak of Na-birnessite is 44% relative to the strongest (111) peak. For the synthetic birnessite, on the other hand, the (001) peak height is about 36% relative to the (111) peak, which is close to the theoretical value. In addition, the (001) peak of the embedded particles is more broadened, having a FWHM of about 0.06 $Å^{-1}$ compared to about 0.02 $Å^{-1}$ for synthetic Na-birnessite. Although it is well-established that a decreased particle size results in broadened diffraction peaks, in this case, however, the particle size alone cannot account for the broadness of the (001) peak. Assuming that the embedded particles are perfectly ordered, the estimated particle size based on the Scherrer equation is less than 1.5 nm. This value is much smaller than the particles size (∼10 nm) observed in Fig. 1(b). Hence this strongly suggests that structural disorder is largely responsible for the broadening and weakened (001) peak.

We have conducted electron scattering simulations to model the effects of different types of the structural disorder, including the size effect, layer mis-registration and Mn vacancies, to the CDI (simulation details can be found in the Supporting Information). The comparisons between the experimental and theoretical CDI is intended to be qualitative, as the presence of dynamical scattering in electron diffraction means that quantitative agreement (matching peak heights) can be achieved only under very specific experimental conditions (essentially perfect crystals of known thickness and orientation). In our case we make a qualitative comparison of the apparent trend and features in the experimental CDI. As shown in Fig. 3, the effect of nano-sized particles, as expected, caused a slight broadening to all diffraction peaks (black line). However, the inclusion of Mn vacancies and layer mis-registrations, result in a pronounced change, particularly to the (001) peak. It can be seen that the presence of a high concentration of the Mn vacancies drastically reduce the intensity of the (001) peak but the width of the (001) peak remains unchanged from that observed for the ordered particles. The higher-order peaks remain relatively unchanged. On the other hand, the presence

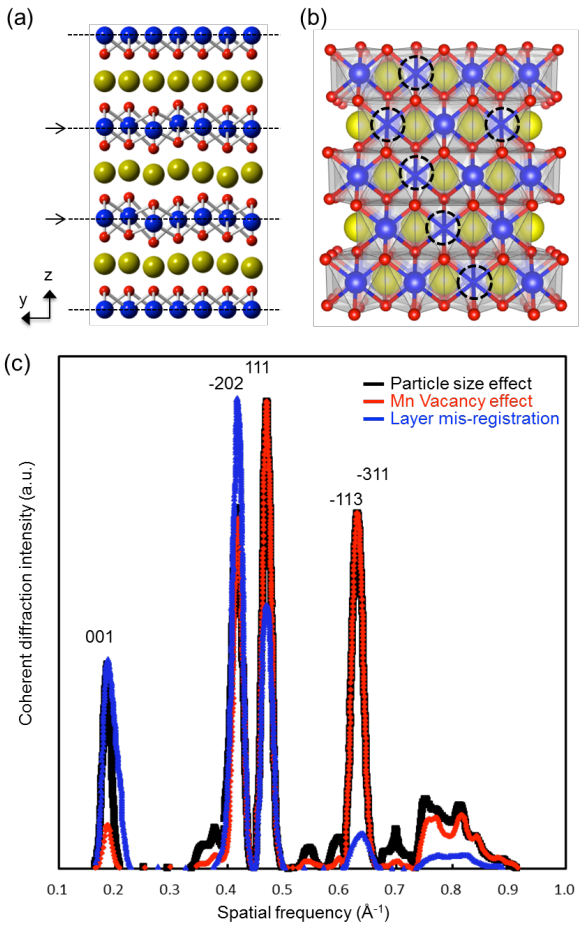

Fig. 3 Schematic diagrams of the types of disorders in birnessite: (a) layer mis-registration and (b) Mn vacancies, with vacancies represented by dashed circles; and (c) the simulated electron diffraction intensities of 10 nm size spherical particles (black), particles with 40% Mn vacancies (red) and particles with layer mis-registration (blue).

of layer mis-registration, even with an average deviation of only 0.1 Å in our simulation, result in a further assymmetric broadening of the (001) peak, and a drastic reduction to the $(\bar{1}33)/(\bar{3}11)$ peaks (and higher-order), but does not drastically change the relative heights of the other major peaks, $(\bar{2}02)$ and (111). The combined effects of Mn vacancies and layer mis-registration agree with the trend observed in the experimental CDI of the particles in Nafion.

Our simulation results suggest that the strongly reduced intensity and broadening of the (001) peak, and the greatly damped intensity of the $(\bar{1}33)/(\bar{3}11)$ peaks, arises from mis-registration of the layer stacking and a high concentration of Mn layer vacancies in the embedded birnessite particles. These structural disorder features have an effect on the cat-

alytic activities of the birnessite phase particles. For example, similar (001) diffraction features have also been observed in the birnessite phase solids formed from biogenically produced manganese oxides[29,30]. Such structural features in the biogenic oxide was believed to be the result of the fast oxidation of Mn^{II} to form Mn^{III}/Mn^{IV} oxides in mild conditions. In addition, a high concentration of Mn layer vacancies has significant consequences for the activity of photo-electrochemical water-oxidation catalysis. The MnO_6 octahedron have been shown experimentally and theoretically to be less compressed (more elongated octahedral) compared to vacancy-free birnessite[26,31,32], indicating an increase of weaker, more flexible Mn-O bonds. This is also in agreement with spin-polarised DFT calculations[26]. The presence of flexible Mn-O bonds has been correlated with higher water-oxidation activity[15]. Moreover, a high concentration of Mn vacancies can greatly reduce the band gap, implying an improved light absorption efficiency. Overall, the layer mis-registration and Mn vacancies that we have observed in this system provide a change in the atomic and electronic structures from the ideal, perfect manganese oxide crystal structure, leading to an improved efficiency in both water-oxidation and photo-reduction.

The authors acknowledge the use of facilities at the Monash Centre for Electron Microscopy and the Australian Synchrotron XAS beam line. The authors would also like to thank the Australian Research Council for financial support provided through the ARC Centre of Excellence for Electromaterials Science (ACES).

References

1 Y. Umena, K. Kawakami, J. R. Shen and N. Kamiya, *Nature*, 2011, **473**, 55.
2 R. Brimblecombe, G. C. Dismukes, G. F. Swiegers and L. Spiccia, *Dalton Trans.*, 2009, 9374.
3 R. Cao, W. Lai and P. Du, *Energy Environ. Sci.*, 2012, **5**, 8134.
4 A. Sartorel, M. Carraro, F. M. Toma, M. Prato and M. Bonchio, *Energy Environ. Sci.*, 2012, **5**, 5592.
5 M. Dinca, Y. Surendranath and D. G. Nocera, *Proc. Natl. Acad. Sci. USA*, 2010, **107**, 10337.
6 A. Singh, S. L. Y. Chang, R. K. Hocking, U. Bach and L. Spiccia, *Energy Environ. Sci.*, 2013, **6**, 579.
7 A. Kay, I. Cesar and M. Gratzel, *J. Am. Chem. Soc.*, 2006, **15**, 15714.
8 V. Artero, M. Charvarot-Kerlidou and M. Fontecave, *Angew. Chem. Int. Ed*, 2011, **50**, 7238.
9 F. Jiao and H. Frei, *Energy Environ. Sci.*, 2010, **3**, 1018.
10 M. Morita, C. Iwakura and H. Tamura, *Electrochim. Acta*, 1977, **23**, 331.
11 Y. Gorlin and T. F. Jaramillo, *J. Am. Chem. Soc.*, 2010, **132**, 13612.
12 A. M. Mohammad, M. I. Awad, M. S. El-Deab, T. Okajima and T. Ohsaka, *Electrochim. Acta*, 2008, **53**, 4351.
13 R. N. Singh, J. P. Singh, H. N. Cong and P. Chartier, *Int. J. Hydrogen Energy*, 2006, **31**, 1372.
14 T. Takashima, K. Hashimoto and R. Nakamura, *J. Am. Chem. Soc.*, 2012, **134**, 1519.
15 D. M. Robinson, Y. B. Go, M. Mui, G. Gardner, Z. Zhang, D. Mastrogiovanni, E. Garfunkel, J. Li, M. Greenblatt and G. C. Dismukes, *J. Am. Chem. Soc.*, 2013, **135**, 3494.
16 A. Singh, R. K. Hocking, S. L. Y. Chang, B. M. George, M. Fehr, K. Lips, A. Schnegg and L. Spiccia, *Chem. Mater.*, 2013, **25**, 1098.
17 P. Zaharieva, I.and Chernev, M. Risch, K. Klingan, M. Kohlhoff, A. Fischer and H. Dau, *Energy Environ. Sci.*, 2012, **3**, 2330.
18 V. B. R. Boppana and F. Jiao, *Chem. Commun.*, 2011, **47**, 8973.
19 M. Fekete, R. K. Hocking, S. L. Y. Chang, C. Italiano, T. A. Patti, F. Arenae and L. Spiccia, *Energy Environ. Sci.*, 2013, **6**, 2222.
20 M. M. Najafpour, T. Ehrenberg, M. Wiechen and P. Kurz, *Angew. Chem., Int. Ed.*, 2010, **49**, 2233.
21 Y. Hsu, Y. Chen, Y. Lin, L. Chen and K. Chen, *J. Mater. Chem.*, 2012, **22**, 2733.
22 N. Sakai, Y. Ebina, K. Takada and T. Sasaki, *J. Phys. Chem. B*, 2005, **109**, 9651.
23 R. K. Hocking, R. Brimblecombe, S. L. Y. Chang, A. Singh, M. H. Cheah, C. Glover, W. H. Casey and L. Spiccia, *Nature Chemistry*, 2011, **3**, 461.
24 D. M. Robinson, Y. B. Go, M. Greenblatt and G. C. Dismukes, *J. Am. Chem. Soc.*, 2010, **132**, 11467.
25 A. Iyer, J. Del-Pilar, C. K. King, E. Kissel, H. F. Garces, H. Huang, A. M. El-Sawy, P. K. Dutta and S. L. Suib, *J. Phys. Chem. C*, 2012, **10**, 6474.
26 K. D. Kwon, K. Refson, and G. Sposito, *Phys. Rev. Lett.*, 2008, **100**, 146601.
27 M. Wiechen, I. Zaharieva, D. Holger and P. Kurz, *Chem. Sci.*, 2012, **3**, 2330.
28 J. Parant, R. Olazcuaga, M. Devalette, C. Fouassier and P. Hagenmuller, *J. Sol. Stat. Chem.*, 1971, **3**, 1.
29 M. Villalobos, B. Toner, J. Bargar and G. Sposito, *Geochim. Cosmochim. Acta*, 2003, **67**, 2649.
30 M. Villalobos, B. Lanson, A. Manceau, B. Toner and G. Sposito, *Am. Mineral.*, 2006, **91**, 489.
31 A. C. Gaillot, D. Flot, V. A. Drits, A. Manceau, M. Burghammer and B. Lanson, *Chem. Mater.*, 2003, **15**, 4666.
32 I. Djerdj, D. Arcon, Z. Jaglicic and M. Niederberger, *J. Phys. Chem. C*, 2007, **111**, 3614.